Materials Science & Engineering A 707 (2017) 426–434

Contents lists available at ScienceDirect

Materials Science & Engineering A

journal homepage: www.elsevier.com/locate/msea

Improving joint performance of friction stir welded wrought Mg alloy by controlling non-uniform deformation behavior

Q. Shang[a,b], D.R. Ni[a,*], P. Xue[a], B.L. Xiao[a], Z.Y. Ma[a,*]

[a] Shenyang National Laboratory for Materials Science, Institute of Metal Research, Chinese Academy of Sciences, 72 Wenhua Road, Shenyang 110016, China
[b] School of Materials Science and Engineering, University of Science and Technology of China, 72 Wenhua Road, Shenyang 110016, China

ARTICLE INFO

Keywords:
Non-uniform deformation
Mg alloy
Friction stir welding
Mechanical properties
Texture evolution
Twinning

ABSTRACT

Macroscopic non-uniform deformation is usually found in deformed joints of friction sir welded (FSW) wrought Mg alloys, detrimental to the joint performance. In the present work, two kinds of FSW joints with different stirred zone (SZ) structures were generated for extruded AZ31 plates. Comparative studies were conducted aiming to unravel the underline mechanism of the non-uniform deformation and their effect on tensile properties. It was found that the occurrence of non-uniform deformation was associated with the special texture distribution and twinning behavior in the SZ. The shape of concave sub-regions in the SZ coincided with the distribution area of extension twins. Texture evolution showed that consistent lattice rotation occurred across the SZ during tensile process. Schmid factor analysis revealed the role acted by basal slip and extension twinning in sub-regions at various deformation stages. In addition, the non-uniform deformation behavior could be suppressed by modifying the texture distribution through increasing the tool rotation rate, which meanwhile could improve both the tensile strength and ductility of the joints. Digital image correlation measurements provided detailed examination of the actual strain distribution evolved in the joints and demonstrated the dominant contribution of strain localization to the tensile properties.

1. Introduction

With significant superiority in weight reduction for energy saving, light structural materials like Mg alloys have aroused increasing research attention for industrial application. The extensive utilization of Mg alloys necessitates the selection of reliable welding techniques to achieve sound joints with mechanical predominance. Friction stir welding (FSW), as a solid state joining method, has been proved to be quite workable to obtain ideal welds with fine and equiaxed grains [1–3]. Despite the microstructure optimization, specific texture distribution was inevitably introduced in the stirred zone (SZ) [4–6]. Previous studies have confirmed the significant effect of the texture induced strain localization on the mechanical behavior of FSW Mg alloys [7–12]. It was suggested that premature cracks preferentially initiate in the regions subjected to severe deformation concentration and deteriorate the joint performance. Accordingly, it is essential to promote understanding about the non-uniform deformation and unravel the underline mechanism.

Some investigations have manifested the common occurrences of non-uniform macroscopic deformation in FSW Mg joints when subjected to various loading paths, like transverse tension and compression [13,14], bending [15,16], and stress fatigue [17]. Similar "concave-convex" appearances could be found on the cross-sectional surfaces of the FSW joints enduring different loading methods. Yang et al. [17] recognized it as the consequence of the grain orientation distribution and shear layers arrangement but no detailed analysis provided. He et al. [18,19] used a multi-scale model to simulate the strain localization, finding that slips and twinning took the dominant roles in different sub-regions. However, the simplified model adopted still lacks authenticity in describing the actual deformation characteristics. Furthermore, it was seldom discussed in regarding reports that the twinning area would evolve in different deformation stages, thus the contribution of twinning was usually underestimated. In addition, the texture evolution stemmed from both the slip induced lattice rotation and twinning reorientation in the deformation process could also complicate the problem, giving rise to the need for further investigation.

Although FSW joints of wrought Mg alloys usually showed lower tensile properties than the base metal (BM), some prior works on FSW AZ31 indicated that the joint efficiency could be enhanced by increasing the rotation rate [20–22]. Yang et al. [21] achieved an excellent joint efficiency up to 95% by increasing the rotation rate and

* Corresponding authors.
E-mail addresses: drni@imr.ac.cn (D.R. Ni), zyma@imr.ac.cn (Z.Y. Ma).

http://dx.doi.org/10.1016/j.msea.2017.09.084
Received 27 July 2017; Accepted 19 September 2017
Available online 20 September 2017
0921-5093/

found that the SZ evolved from an elliptical nugget to a two-layer structure. Through comparative study on the non-uniform deformation and mechanical behavior of two AZ31 FSW joints with different SZs, the current work was designed to uncover the intuitive correlation between the SZ structure and the non-uniform deformation behavior and its effect on mechanical properties. Detailed analysis was also conducted to experimentally verify the underline mechanism of the non-uniform deformation characteristics.

2. Experimental

In this study, as-extruded AZ31 plates with a thickness of 6.4 mm were used as BM. Bead-on-plate welding was conducted with the welding direction perpendicular to the extrusion direction. A steel tool with a concave shoulder of 24 mm in diameter and a threaded cylindrical pin of 8 mm in diameter and 5.8 mm in length was adopted. Two rotation rates (800 rpm and 2000 rpm) at a certain speed of 100 mm min^{-1} were applied to obtain two typical SZ structures, and the joints were correspondingly denoted as 800 rpm-joint and 2000 rpm-joint.

Optical microscope (OM) and electron backscattered diffraction (EBSD) were used to characterize and analyze the microstructure and texture evolution. Samples for OM observation were cut perpendicular to the welding direction and etched by a solution of 4.2 g picric acid + 70 mL ethanol + 10 mL distilled water + 10 mL glacial acetic acid. EBSD analysis was conducted by a field emission scanning electron microscope (FESEM, Supra 55) equipped with an EBSD detector and an HKL Channel 5 System. Samples for EBSD analysis were prepared by electropolishing using the 10% perchloric acid ethanol solution.

Tensile specimens with a parallel section of 40 × 10 × 6 mm were electrical discharge machined perpendicular to the welding direction. All tensile tests were carried out at a strain rate of $1 \times 10^{-3}\ s^{-1}$ on a Zwick/Roell Z050 tester, and each test was repeated three times. To characterize the microstructure evolution, additional tensile tests were performed up to different stress levels of 100 MPa and ~ 90% ultimate tensile strength (UTS), i.e., 200 MPa for 800 rpm-joint and 220 MPa for 2000 rpm-joint. After tension to ~ 90% UTS, the contour profiles were measured on the non-uniformly deformed surfaces of the joints using a 3D optical scanner. To evaluate the local strain distribution, the digital image correlation (DIC) technique was employed using a commercial GOM ARAMIS DIC system [14,23].

3. Results

3.1. Microstructure and texture

Fig. 1 shows the macroscopic images of the FSW AZ31 joints. The SZ of 800 rpm-joint exhibited a large elliptical shape. At a higher rotational rate of 2000 rpm, the SZ turned out to be a two-layer structure, i.e. the triangular upper SZ (denoted as USZ) and elliptical lower SZ (denoted as LSZ). Specifically, the thickness of the USZ is approximately equivalent to that of the LSZ. The optical micrographs of the SZs are given in supplementary Fig. S1.

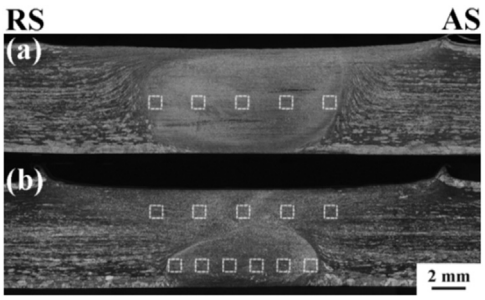

Fig. 1. Macroscopic images of cross-sections of FSW AZ31 joints: (a) 800 rpm-joint and (b) 2000 rpm-joint.

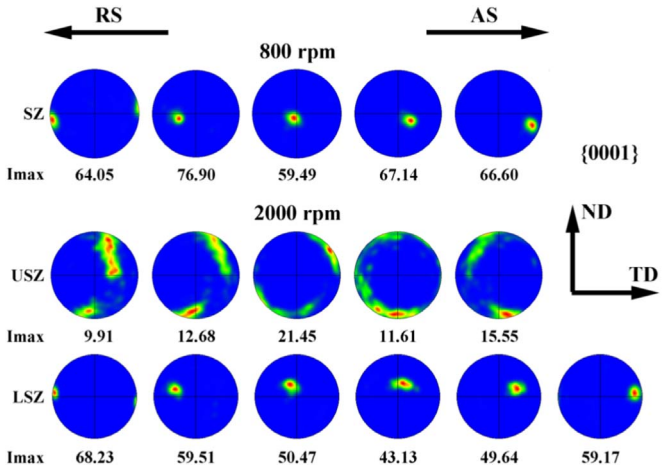

Fig. 2. {0001} pole figures of different regions in SZ of 800 rpm-joint and 2000 rpm-joint. (The measurement locations are indicated in Fig. 1).

The texture distribution investigated by EBSD across the SZs of the two joints was illustrated in Fig. 2. It is noted that a typical characteristic of texture distribution appeared in the SZ of 800 rpm-joint with the poles of c-axes gradually rotating from the transverse direction (TD) to the welding direction (WD) as the position moving from SZ-boundaries to SZ-center. For the 2000 rpm-joint, the USZ and LSZ exhibit entirely different texture types. The texture distribution in the LSZ is similar to that in the 800 rpm-joint while the texture in the USZ is much more complicated. Compared to the strong texture evolved in the 800 rpm-joint, the texture in the USZ of the 2000 rpm-joint is significantly randomized with drastically eclipsed intensity even though some texture components exhibit an alignment of c-axes close to the normal direction (ND); besides, no obvious regularity was found in the texture distribution across the USZ, implying a complicated material transportation in such region during FSW.

3.2. Tensile behavior

Table 1 summarizes the transverse tensile properties of the BM and FSW joints. The associated engineering stress-strain curves are presented in supplementary Fig. S2. It was revealed that the yield strengths (YS) of the FSW joints were obviously lower than that of BM. In addition, both the UTS and elongation (El) of the 2000 rpm-joint are higher than those of the 800 rpm-joint. It is noted that the joint efficiency (defined as the ratio of UTS between the joint and the BM) was optimized from 92.2% to ~100% and the El was enhanced from 7.3% to 10.5%.

3.3. Non-uniform macroscopic deformation

As revealed in Fig. 3, severe non-uniform deformation occurred in both FSW joints after transverse tensile tests. The overall deformation appearances varied with different rotation rates but similar “concave-convex” regions were obtained in the surface on the TD-ND plane. The whole SZ of 800 rpm-joint exhibited a “concave-convex” appearance while such morphology only arose at the LSZ of the 2000 rpm-joint.

Table 1
Transverse tensile properties of as-extruded AZ31 and FSW joints.

	YS, MPa	UTS, MPa	El, %	Joint efficiency, %
BM	158 ± 5.0	243 ± 2.6	12.8 ± 0.9	
800 rpm-joint	96 ± 6.4	224 ± 0.4	7.3 ± 1.1	92.2
2000 rpm-joint	99 ± 8.1	242 ± 6.6	10.5 ± 0.7	99.6

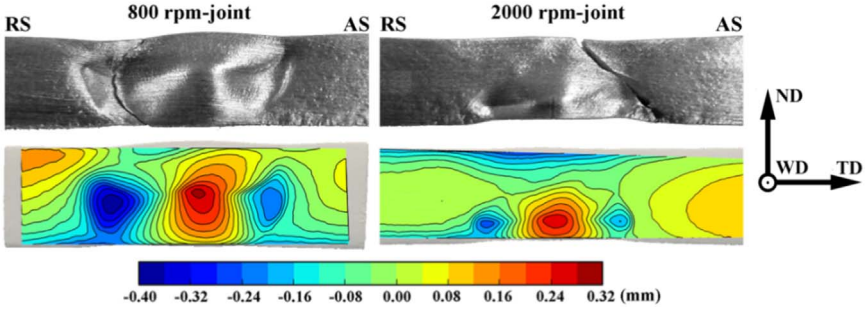

Fig. 3. Deformation morphology of failed FSW joints and contour profiles of joints tensiled up to ~ 90% UTS.

Accordingly, the "concave-convex" regions were conjectured to relate to the elliptical structures in both the joints and the contour edges were consistent with the SZ boundaries. It is noted that materials at the center of the concave-convex regions would protrude along the WD without obvious deformation appearing on the reverse side. On the bulge side, a couple of concave sub-regions in a fan shape were distributed roughly symmetric between the advancing side (AS) and the retreating side (RS). For the samples subjected to transverse tension, the concave regions are actually the places where deformation mainly concentrated. Besides, the area and the concavity of the concave sub-regions on the RS are greater than that on the AS, revealing some asymmetry in plastic deformation.

3.4. Microstructure evolution in tensile deformation

Fig. 4 exhibits the microstructure evolution in the 800 rpm-joint when deformed to different stress levels. At the stress of 100 MPa, twins were observed initiating near the SZ-boundaries due to the favorable orientation. It was verified in Fig. 2 that the (0001) basal planes of grains adjacent to SZ-boundaries were roughly perpendicular to the tensile direction, leading to a preferential activation of {10-12} < 10-11 > extension twins. When the stress was enhanced up to 200 MPa, the twin volume fraction increased significantly near the boundaries and the twinning area propagated from the boundaries to the SZ-center. As illustrated in Fig. 5, the shape of twinning area in the SZ of 800 rpm-joint was approximately triangular, roughly coinciding with the shape of concave sub-regions (Fig. 3). Similar phenomenon was also observed in the LSZ of 2000 rpm-joint.

4. Discussion

4.1. Microstructure and texture evolution

The influence of welding parameters on the heat input has been considerably investigated before. According to the study by Arbegast et al. [24], the relationship between the welding parameters and the peak temperature in a SZ was given in Eq. (1):

$$\frac{T}{T_m} = K\left(\frac{W^2}{V \cdot 10^4}\right)\alpha \tag{1}$$

where T_m is the melting point of the alloy, and α and K are constants. The W and V represent the rotation rate and welding speed, respectively. It is confirmed by the equation that higher heat input can be obtained with the increase of rotation rate.

In this regard, the SZ shape evolution could be deduced to be related to the reinforced effect of shoulder with increasing rotation rate. As reported by relevant literatures [25–27], the shoulder usually takes the dominant role in heat generation and the temperature gradually goes down from the weld top to the bottom. Therefore, with the increasing temperature induced by rotation rate enhancement, growing amount of materials beneath the shoulder are softened and the plasticized region complied with the shoulder driving force would expand downwards. Consequently, the prevailing impact of pin on material flow would be suppressed by the stepped-up prominence of shoulder. Also, the shape

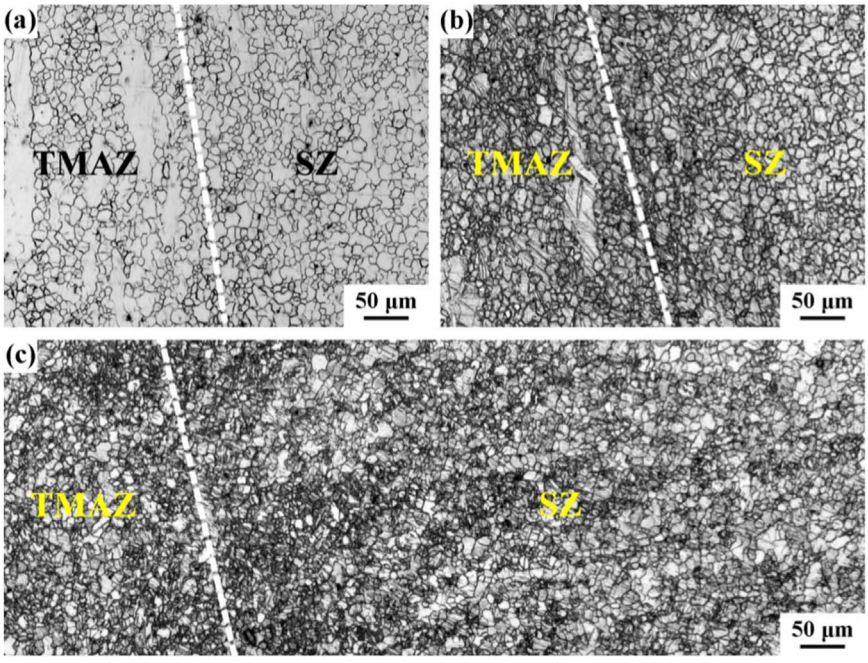

Fig. 4. Microstructure near SZ-boundary on RS in 800 rpm-joint at different stress stages: (a) 0 MPa, (b) 100 MPa, and (c) 200 MPa.

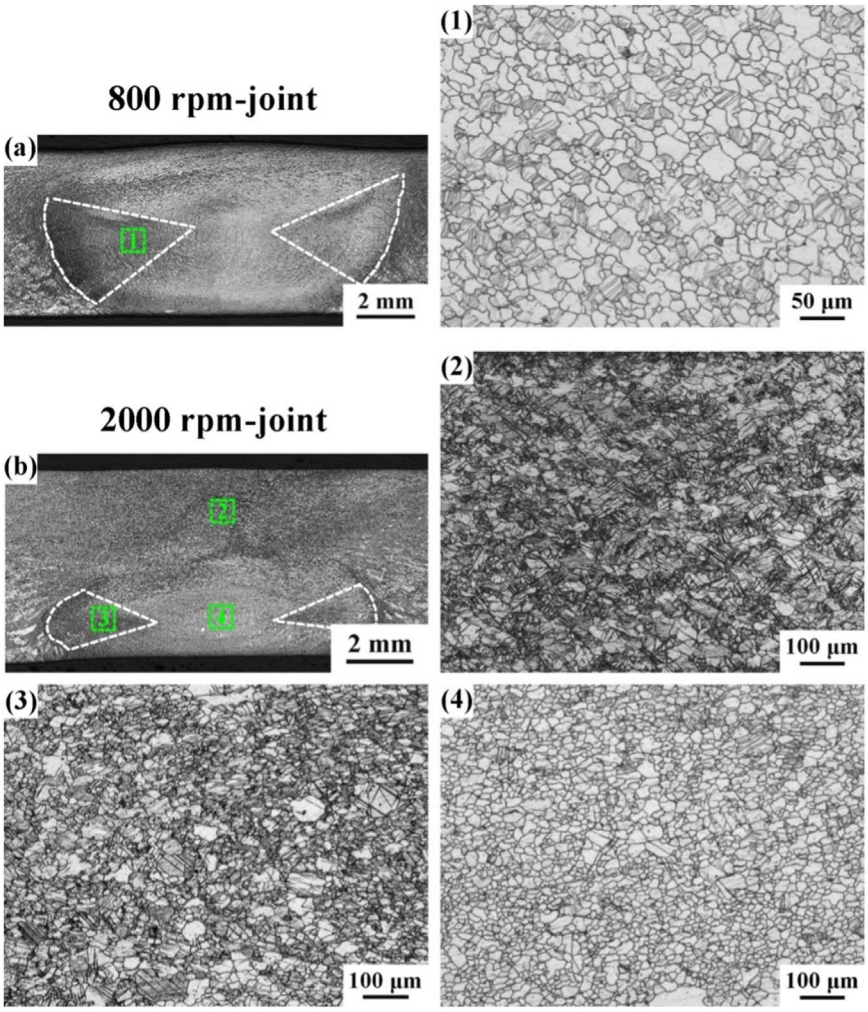

Fig. 5. Macro and micro metallographs of FSW AZ31 joints tensiled up to ~ 90% UTS: (a) 800 rpm-joint and (b) 2000 rpm-joint (The contour of twinning area is highlighted with dashed white lines. The locations of micrographs are marked with green wireframes.). (For interpretation of the references to color in this figure legend, the reader is referred to the web version of this article.)

of the USZ would be consistent with the volumetric distribution of temperature field.

As deformation textures are usually imposed on resultant microstructure after plastic flow, the difference in texture evolution between the two types of joints could be related to the different modes of material flow. The formation of texture in 800 rpm-joint could be simply considered as the result of an extrusion process. It was reported by Krishnan [28] that the FSW process could be thought of as simply extruding one semi-circular shear layer in one rotation of the tool. Park et al. [4] found that the formation and the repetitive stacking of these shear layers would give rise to an intense (0001) basal plane texture as only the basal slip systems preferentially operated during the welding. Suhuddin et al. [29] also confirmed the material flow as a complex process mainly associated with the basal slip.

In case of the 2000 rpm-joint, the flow pattern is quite different due to the growing effect of shoulder and the hierarchical process of the SZ, which agrees well with the flow-partitioned model proposed by Arbegast [30]. Although the texture distribution developed in the LSZ indicates similar layered material flow with that in the 800 rpm-joint, the randomized texture components in the USZ can reveal considerably turbulent and complicated plastic deformation. As reported by Kumar et al. [31], unlike the pin that can transfer the material layer by layer, the shoulder could just provide a shear stress to transport the material bulk. The diminishing of such stress with increasing distance from shoulder makes it impossible to achieve the extruded shear layers with strong texture. In addition, the mixing of material flow induced simultaneously by the shoulder and pin in the USZ also complicates the texture evolution.

4.2. Non-uniform deformation behavior

4.2.1. Different deformation characteristics between the two types of joints

As shown in Fig. 3, severe incompatible deformation occurred in the different sub-regions of SZ after transverse tensile test and significant difference can be observed between the two types of joints. For the 800 rpm-joint, the whole SZ exhibited a concave-convex morphology. For the 2000 rpm-joint, in contrast, such phenomenon only appeared in the LSZ while no severe incompatible deformation occurred in the USZ. As the activation of various deformation modes at ambient temperature is usually governed by the local texture, this difference in deformation behavior could result from the discrepancy in texture characteristics.

From the pole figures shown in Fig. 2, it is evident that the concave-convex appearance should be related to the specifically distributed strong texture existed in both the SZ of 800 rpm-joint and the LSZ of 2000 rpm-joint. The great microtexture difference in various sub-regions could give rise to the different involvement of (0001) basal slip and {10-12} < 10-11 > extension twinning, which are predominantly operative in ambient temperature as the critical resolved shear stress (CRSS) required for them are much lower than that for non-basal slips and other twinning systems [32,33]. Simply, the basal slip and {10-12} twinning would take different roles in different sub-regions. For the basal slip, the grain orientations in the SZ-center and the regions near boundaries are quite hard and the Schmid factor (SF) for transverse tensile load would increase first and then decrease as moving away from boundaries to center, meaning that the basal slip tends to concentrate in the area between SZ-center and SZ-boundaries.

Unlike basal slip which is non-directional, the SF for {10-12}

twinning can be quite different for tensile and compressive stress because of the polar characteristic of twinning shear. Therefore, the extension along c-axis is quite favorable for {10-12} twinning while compression along c-axis adds considerable impediment to its activation. It could thus be inferred that the SF for {10-12} twinning would gradually go down from SZ-boundaries to SZ-center due to the deviation of tensile load direction from c-axes. Consequently, {10-12} twin would preferentially initiate near the SZ-boundaries and gradually expand to the SZ-center with the increase of stress level during the tensile process. It is the different contribution of the basal slip and the extension twinning to deformation that would give rise to the strain localization, leading to the concave-convex appearance in these places.

Compared with the specific strong texture evolved in the LSZ, the texture in the USZ was significantly weakened and randomized, thereby effectively avoiding the site-specific selection of certain deformation modes; that is to say, the basal slip and twinning would not preferentially concentrate in specific sub-regions, thus inhibiting the occurrence of strain localization and homologous incompatible deformation.

4.2.2. Twinning area and the concave appearance

As seen in Fig. 5, the triangular shaped concave regions approximately coincide with the distribution area of twins at nearly the end of the tensile testing. Although twinning was usually reported to be less contributive to the whole strain owing to the low twinning shear of {10-12} twins in magnesium ($\gamma_t = 0.13$), these observations reveal the non-negligible role of twinning in the deformation of FSW joints. The additional strain induced by twinning leads to the deformation localization in these twin-distributed sub-regions. Therefore, the shape of the concave regions can be explained by verifying the distribution characteristics of twins during tensile deformation.

The special distribution of twins is speculated to be determined by the global distribution of microtexture on the cross sections of the joints, which is determined by the repetitive stacking of shear layers during FSW. In view of this, a grain orientation distribution model is proposed in the present study aiming to explain the characteristics of twin propagation and distribution. Several basic assumptions are listed as follows to simplify the model and the analysis process:

(1) The distribution of basal planes in resultant microstructure entirely aligns with the geometry of shear layers.
(2) The inclination of tool is ignored to prevent the shear layers from the downward and backward forging effect so that the geometry of shear layers is circular around the normal direction. The difference between the AS and RS is also neglected.
(3) The rotation of grains during tension is ignored that the grain orientations can remain unchanged until the twins formed.
(4) The distance between SZ-center and SZ-boundaries is a function of depth. The geometry of a shear layer is the curved face formed by the rotation of the SZ-boundary line.

As indicated in Fig. 6, the function of SZ-boundary line can be set by Eq. (2):

$$y = f(x),\ f(x) \geq 0 \tag{2}$$

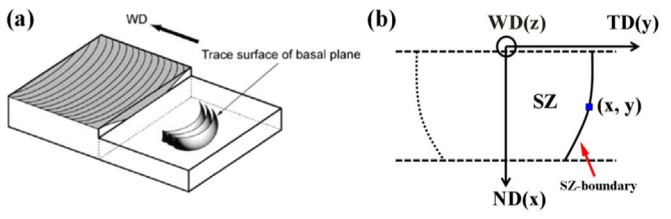

Fig. 6. Schematic illustrations of (a) trace surface of basal plane [4] and (b) function of SZ-boundary.

Let the curve rotate around axis x, the function of the curve surface is shown in Eq. (3) :

$$F(x, y, z) = f^2(x) - y^2 - z^2 \tag{3}$$

Thus, the normal vector of the surface can be described by Eq. (4)

$$(F'_x(x, y, z), F'_y(x, y, z), F'_z(x, y, z)) = (-2f(x)\cdot f'(x), 2y, 2z) \tag{4}$$

The included angle between the normal and the tensile direction (0,1,0) can be calculated by Eq. (5)

$$\cos\alpha = \frac{y}{f(x)\sqrt{[f'(x)]^2 + 1}} \tag{5}$$

The criterion for twinning is confirmed by Eq. (6)

$$\sigma \cos\alpha \geq \sigma^T_{CRSS} \tag{6}$$

σ^T_{CRSS} is the critical resolved stress required on c-axes to activate {10-12} twins.

$$\text{When}\quad y \geq 0,\ \sigma \geq \frac{\sigma^T_{CRSS}}{y} f(x)\sqrt{[f'(x)]^2 + 1} \tag{7}$$

From formula (7), one can find out that when x is a constant, the stress required for twinning would increase with decreasing y, which is consistent with the observation that the twinning area would expand from SZ-boundaries to SZ-center with increasing stress level during tension.

When σ is a constant, formula (7) can be converted into formula (8)

$$f(x)\sqrt{[f'(x)]^2 + 1} \leq \frac{\sigma}{\sigma^T_{CRSS}} y \tag{8}$$

Thus, the range of x would decrease with decreasing y, which is also consistent with the phenomenon that the range of twinning area in ND would decrease when approaching SZ-center.

Generally, we found that the simplified model was roughly appropriate to describe the distribution characteristics of extension twins and the shape feature of twinning area was closely related to the geometry of shear layers.

4.2.3. Orientation evolution during tensile process

In the tensile deformation process, appreciable numbers of twins would form and cause drastic texture change; for instance, extension twinning could reorient the basal planes for about 86°. In addition, slip induced lattice rotation would also adjust the grain orientations gradually during the continuous deformation. However, the deformation behavior and the metallographic results in the present study indicate that the actual texture evolution was complicated due to the competitive operations between twinning and basal slip as well as their different contribution in various sub-regions. Therefore, the texture distributions at different stages of tension were characterized aiming to figure out the evolution process of grain orientations.

When the 800 rpm-joint was just tensiled to yield at a stress of about 100 MPa (the joint was denoted as 100 MPa-joint), twins could be observed to initiate close to the SZ-boundaries due to the appropriate local texture. Fig. 7 shows the comparative analysis between the 100 MPa-joint and the joint without tension. From the boundary misorientation distributions, a peak at 86 ± 5° appeared in the 100 MPa-joint compared to the control joint, indicating the formation of extension twins. As the extension twinning could reorient the local basal planes for nearly 90°, the texture components introduced by twinning are still unfavorable for basal slip. However, the statistical SF maps indicated that the numbers of grains with high SF for basal slip increased significantly as the stress level up to 100 MPa, implying the effect of slip induced lattice rotation.

It is generally accepted that the slip plane would gradually rotate to parallel with the load direction in the uniaxial tension of a single crystal. In the uniaxial tension of FSW AZ31, the basal planes in different sub-regions of SZ all tend to rotate around the ND and

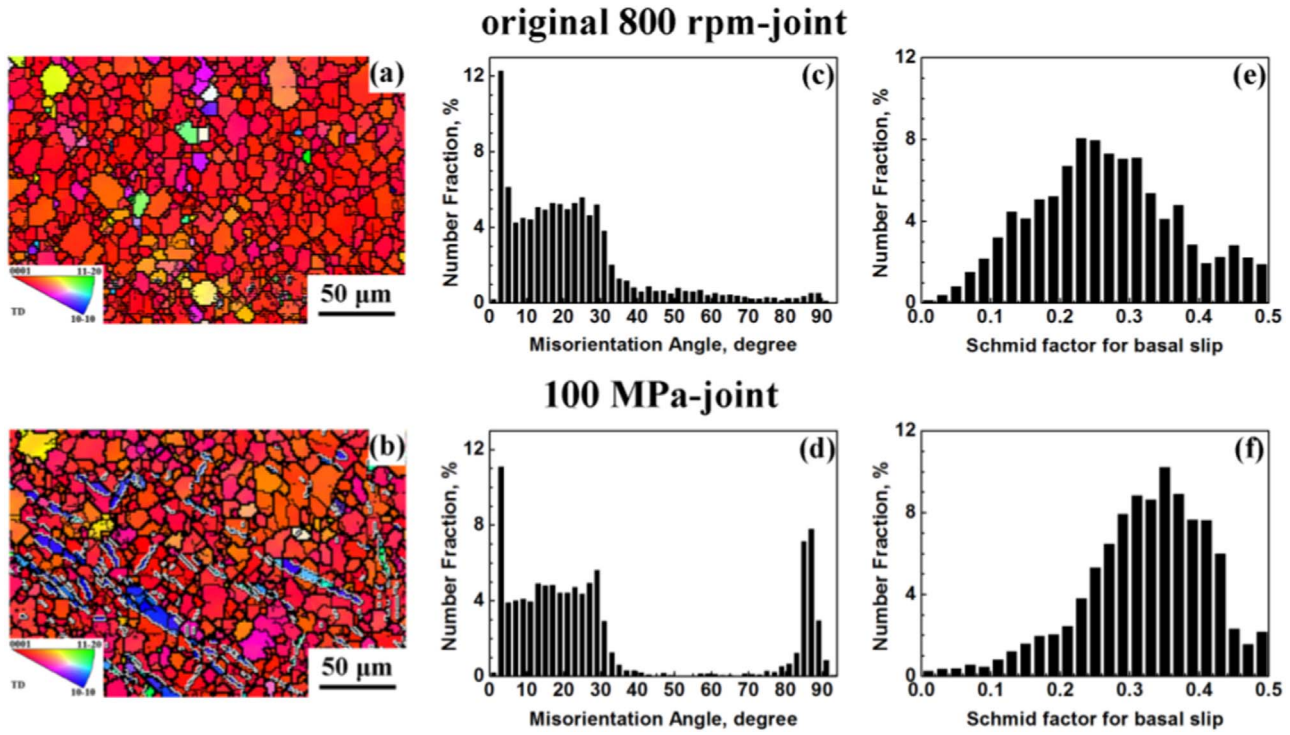

Fig. 7. Comparative analysis between original 800 rpm-joint and 100 MPa-joint at the same place near SZ-boundary: (a) and (b) grain orientation map coded by IPF color, (c) and (d) boundary misorientation distribution, (e) and (f) Schmid factor for basal slip.

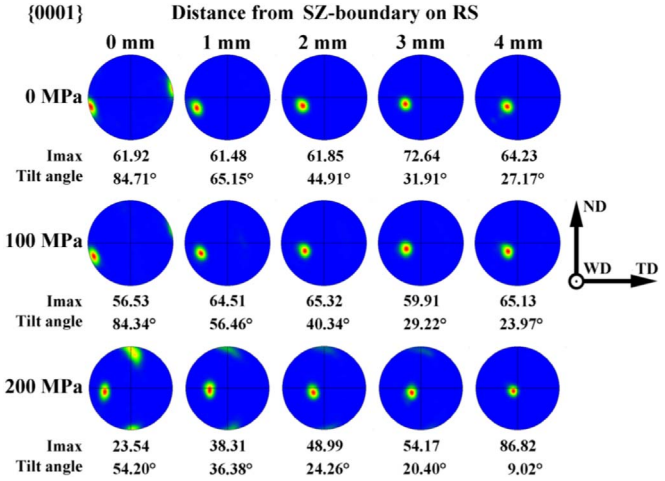

Fig. 8. {0001} pole figures at different regions of 800 rpm-joint at various stress stages. (Tilt angle refers to deviation of max intensity pole from WD).

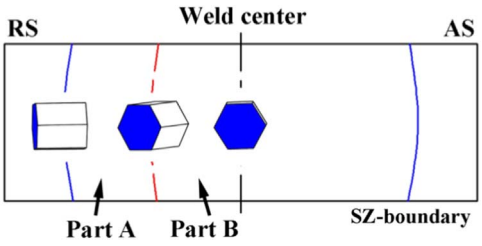

Fig. 9. Schematic illustration for partition of SZ based on texture distribution.

perpendicular to the WD, as exhibited in Fig. 8. This identical lattice rotation in the polycrystalline SZ could be rationalized by the limited slip systems (i.e. basal slip) activated at ambient temperature and the convergent alignment of basal planes among neighboring grains in SZ, demonstrated by the high texture intensity. Due to the lattice rotation, the sub-regions with different initial texture would get geometric hardening or softening. If the angle between the basal plane and TD is more than 45°, the orientation for basal slip would be softened first and then hardened. If not, the orientation would get sustained hardening. From the texture distribution in SZ, the region between SZ-center and SZ-boundary could be divided into two parts as illustrated in Fig. 9. The part near the SZ-boundaries (denoted Part A) would show better continuous deformation capability than the part near the SZ-center (denoted Part B). Fig. 8 shows that the width of Part A in TD is less than 2 mm, hence basal slip would preferentially concentrate in the region very close to the SZ-boundaries.

In addition, the profuse activation of extension twins complicated the actual deformation process, as the introduction of twin lamellae could exert a strengthening effect by grain subdivision and also bring about drastic texture changing. Actually, the introduced texture component is governed by the twin variant selection, which depends on the grain orientations related to the load direction [34]. After tension to 200 MPa, the grain orientations in 800 rpm-joint were characterized and displayed in Fig. 10. It is noted that the twinning induced orientations are similar in different sub-regions. The new texture components are unfavorable for basal slip as the c-axes are all close to the ND. To verify the actual cooperation of twinning and basal slip in the tensile deformation of the strong-textured SZ, the mean SF for both the basal slip and extension twinning in different sub-regions was calculated and shown in Fig. 11. Actually, all the possible basal slip systems and extension twin variants were considered in the calculation and only those with the largest SF were presented. At different stages of tensile deformation, the mean SF for extension twinning would gradually decrease with the position moving from the SZ-boundary to the SZ-center on RS, and that for basal slip would increase first and then decrease. From 0 MPa to 100MPa, the mean SF for extension twinning in all sub-regions would slightly decrease and that for basal slip in the Part A would slightly increase, implying the effect of lattice rotation. From 100 MPa to 200MPa, the mean SF for both extension twinning and basal slip was significantly decreased. This could result from the

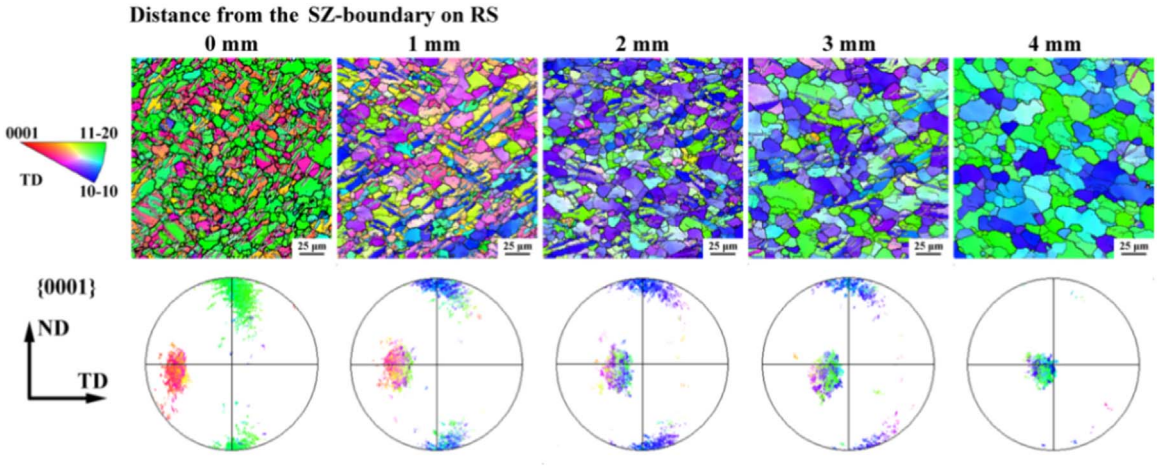

Fig. 10. Grain orientations at different sub-regions in SZ of 800 rpm-joint tensiled up to 200 MPa.

pronounced multiplication of extension twins at that stage, as the texture component introduced by twinning was unfavorable for both twinning and basal slip. In general, local deformation would preferentially concentrate in Part A for its better continuous deformation capability during transverse tension.

4.3. Tensile behavior

As displayed in Table 1, obvious degradation of YS was found in the FSW joints of AZ31 Mg alloy. This could be rationalized by the favorable texture in the region adjacent to the SZ-boundaries where basal slip and extension twinning are preferentially active [8,12]. It was also found that both the UTS and the El were enhanced when the SZ shape evolved from a single nugget to a two layer structure with increasing tool rotation rate. As widely reported that the texture induced strain localization was a critical reason for premature failure in FSW Mg joints [7–14], the improved mechanical performance in the 2000 rpm-joint could be attributed to the relatively uniform deformation. Fig. 3 indicated that both the area size and the altitude variation of the concave-convex region in 2000 rpm-joint were less than those in the 800 rpm-joint, demonstrating inhibited deformation concentration.

However, the intuitive macroscopic deformation can't accurately reflect the actual local strain distribution due to the internal deformation coordination between different sub-regions. With the aim to obtain thorough experimental verification of the difference in strain localization between the two kinds of joints, the distribution of tensile strains at different stress levels was measured via DIC technique and given in Fig. 12. It was observed that strain localization was obviously severer in

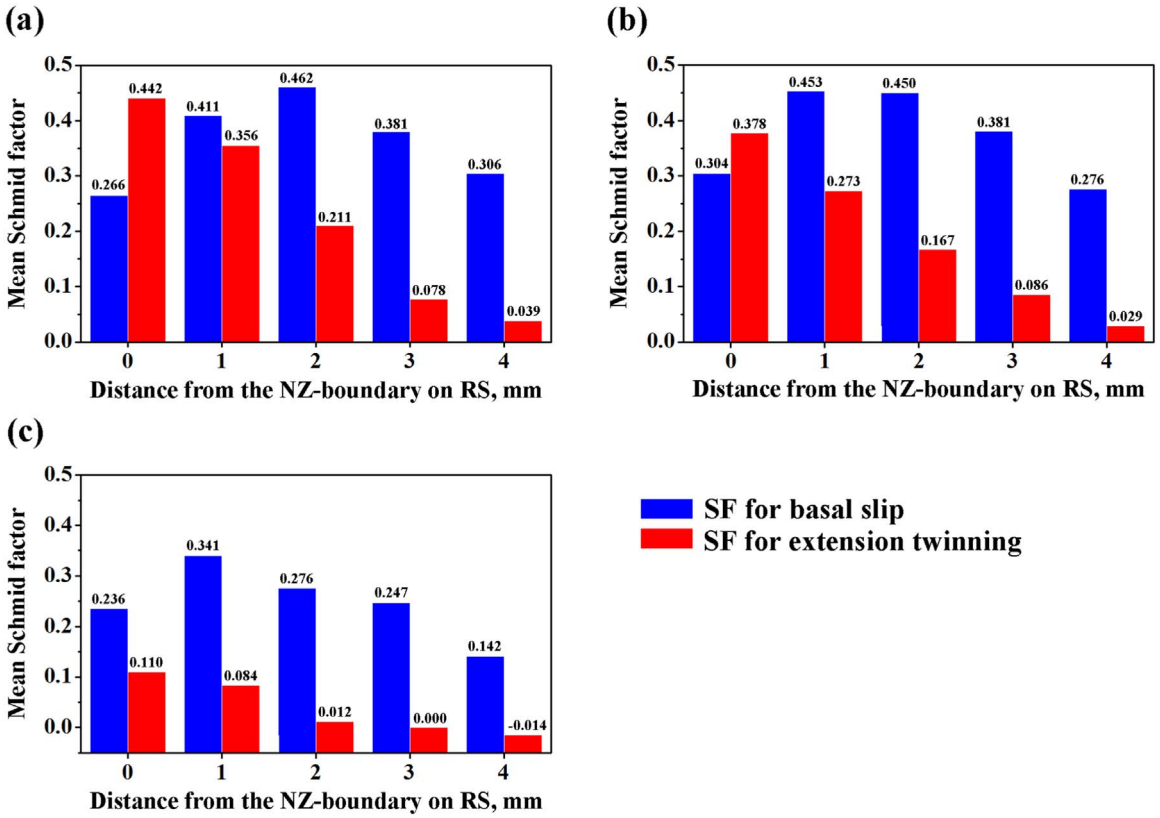

Fig. 11. Mean SFs for basal slip and extension twinning at different sub-regions in the SZ of 800 rpm-joint at the stress levels of (a) 0 MPa, (b) 100 MPa, and (c) 200 MPa.

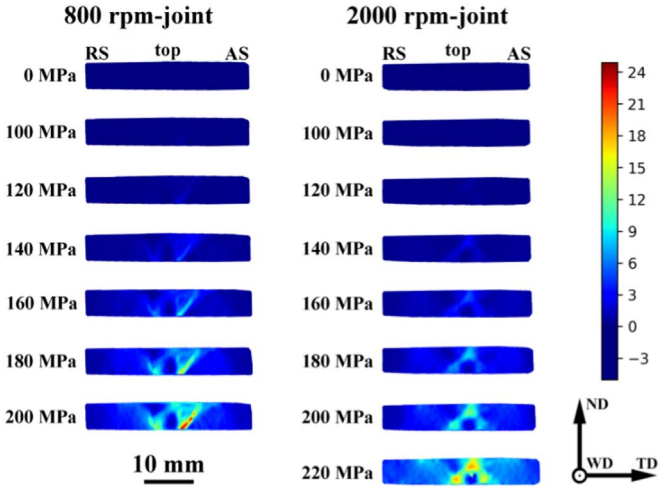

Fig. 12. The distribution of local tensile strains on the bulge sides of 800 rpm-joint and 2000 rpm-joint at different stress levels.

800 rpm-joint at the same stress level. Plastic strains tended to overly concentrate along the SZ-boundary on AS. As for the 2000 rpm-joint, the strain concentration fields were located at the center of USZ and the two sides of LSZ. Specifically, strain distribution in these fields was generally uniform, which in turn postponed the premature failure and thus gave rise to better tensile properties.

Accordingly, it was proved to effectively optimize the joint performance by controlling the strain localization via increasing the tool rotation rate.

5. Conclusions

The non-uniform deformation behavior of typical FSW AZ31 joints during transverse tension was investigated. The underline mechanism of the typical deformation characteristics was uncovered, and the effect of microstructure and texture evolution on deformation behavior and tensile properties was elucidated. Several conclusions are made as follows:

(1) The “concave-convex” appearance in the deformation of FSW AZ31 joints was related to the strong specific-distributed texture with basal planes aligned cycle around the pin column. The area of region with this texture distribution could be reduced by enhancing the tool rotation rate.
(2) The triangular shape of the concave regions was consistent with the distribution area of extension twins. The distribution characteristics of twins could be well explained by a simplified orientation model. Extension twins would be prevalently formed adjacent to the SZ-boundaries.
(3) The consistent lattice rotation induced by basal slip was found in the SZ during the whole tensile deformation process. Thus, the region between the SZ-center and SZ-boundaries could be divided into two parts. Basal slip in the part near the SZ-boundaries would be continuously contributive due to the gradually softened orientation.
(4) The effect of orientation evolution for subsequent deformation was investigated via SF analysis. The results showed that the deformation concentration would occur in the part near SZ-boundaries for the well operation of both slip and twinning.
(5) It is possible to optimize the FSW joint performance of wrought Mg alloys by constraining the strain localization behavior through increasing tool rotation rate.

Author contributions

Q. Shang and D.R. Ni contributed equally to this work, and they conceived the idea and design the experiments. Q. Shang and P. Xue performed the FSW experiments. Q. Shang wrote the paper under the supervision of D.R. Ni, B.L. Xiao and Z.Y. Ma. All authors participated in the data analysis and discussion.

Acknowledgment

This work was supported by the National Natural Science Foundation of China under Grant nos. 51371179 and 51331008.

Appendix A. Supplementary material

Supplementary data associated with this article can be found in the online version at http://dx.doi.org/10.1016/j.msea.2017.09.084.

References

[1] R.S. Mishra, Z.Y. Ma, Friction stir welding and processing, Mater. Sci. Eng. R 50 (2005) 1–78.
[2] C.I. Chang, X.H. Du, J.C. Huang, Achieving ultrafine grain size in Mg–Al–Zn alloy by friction stir processing, Scr. Mater. 57 (2007) 209–212.
[3] E.A. El-Danaf, M.M. El-Rayes, M.S. Soliman, Friction stir processing: an effective technique to refine grain structure and enhance ductility, Mater. Des. 31 (2010) 1231–1236.
[4] S.H.C. Park, Y.S. Sato, H. Kokawa, Basal plane texture and flow pattern in friction stir weld of a magnesium alloy, Metall. Mater. Trans. A 34 (2003) 987–994.
[5] S. Mironov, T. Onuma, Y.S. Sato, H. Kokawa, Microstructure evolution during friction-stir welding of AZ31 magnesium alloy, Acta Mater. 100 (2015) 301–312.
[6] S.H. Chowdhury, D.L. Chen, S.D. Bhole, X. Cao, P. Wanjara, Friction stir welded AZ31 magnesium alloy: microstructure,texture, and tensile properties, Metall. Mater. Trans. A 44A (2013) 323–336.
[7] S.H.C. Park, Y.S. Sato, H. Kokawa, Effect of micro-texture on fracture location in friction stir weld of Mg alloy AZ61 during tensile test, Scr. Mater. 49 (2003) 161–166.
[8] R.L. Xin, B. Li, A.L. Liao, Z. Zhou, Q. Liu, Correlation between texture variation and transverse tensile behavior of friction-stir-processed AZ31 Mg alloy, Metall. Mater. Trans. A 43A (2012) 2500–2508.
[9] R.L. Xin, D.J. Liu, B. Li, L.Y. Sun, Z. Zhou, Q. Liu, Mechanisms of fracture and inhomogeneous deformation on transverse tensile test of friction-stir-processed AZ31 Mg alloy, Mater. Sci. Eng. A 565 (2013) 333–341.
[10] R.L. Xin, D.J. Liu, X.G. Shu, B. Li, X.F. Yang, Q. Liu, Influence of welding parameter on texture distribution and plastic deformation behavior of as-rolled AZ31 Mg alloys, J. Alloy. Comp. 670 (2016) 64–71.
[11] W. Woo, H. Choo, D.W. Brown, P.K. Liaw, Z. Feng, Texture variation and its influence on the tensile behavior of a friction-stir processed magnesium alloy, Scr. Mater. 54 (2006) 1859–1864.
[12] Q. Shang, D.R. Ni, P. Xue, B.L. Xiao, Z.Y. Ma, Evolution of local texture and its effect on mechanical properties and fracture bahavior of friction stir welded joint of extruded Mg-3Al-1Zn alloy, Mater. Charact. 128 (2017) 14–22.
[13] D.J. Liu, R.L. Xin, Y. Xiao, Z. Zhou, Q. Liu, Strain localization in friction stir welded magnesium alloy during tension and compression deformation, Mater. Sci. Eng. A 609 (2014) 88–91.
[14] S. Mironov, T. Onuma, Y.S. Sato, S. Yoneyama, H. Kokawa, Tensile behavior of friction-stir welded AZ31 magnesium alloy, Mater. Sci. Eng. A 679 (2017) 272–281.
[15] D.J. Liu, R.L. Xin, Z.Y. Li, Z. Liu, X. Zheng, Q. Liu, The activation of twinning and texture evolution during bending of friction stir welded magnesium alloys, Mater. Sci. Eng. A 646 (2015) 145–153.
[16] D.J. Liu, R.L. Xin, L.Z. Zhao, Y. Hu, Effect of textural variation and twinning activity on fracture behavior of friction stir welded AZ31 Mg alloy in bending tests, J. Alloy. Compd. 693 (2017) 808–815.
[17] J. Yang, D.R. Ni, B.L. Xiao, Z.Y. Ma, Non-uniform deformation in a friction stir welded Mg–Al–Zn joint during stress fatigue, Int. J. Fatigue 59 (2014) 9–13.
[18] W.J. He, B.F. Luan, R.L. Xin, J.B. Xu, Q. Liu, A multi-scale model for description of strain localization in friction stir welded magnesium alloy, Comput. Mater. Sci. 104 (2015) 162–171.
[19] W.J. He, L. Zheng, R.L. Xin, Q. Liu, Microstructure-based modeling of tensile deformation of a friction stir welded AZ31 Mg alloy, Mater. Sci. Eng. A 687 (2017) 63–72.
[20] L. Commin, M. Dumont, J.-E. Masse, L. Barrallier, Friction stir welding of AZ31 magnesium alloy rolled sheets: influence of processing parameters, Acta Mater. 57 (2009) 326–334.
[21] J. Yang, D. Wang, B.L. Xiao, D.R. Ni, Z.Y. Ma, Effects of rotation rates on microstructure, mechanical properties, and fracture behavior of friction stir-welded (FSW) AZ31 magnesium alloy, Metall. Mater. Trans. A 44A (2013) 517–530.
[22] X.H. Wang, K.S. Wang, Microstructure and properties of friction stir butt-welded AZ31 magnesium alloy, Mater. Sci. Eng. A 431 (2006) 114–117.
[23] C. Leitão, I. Galvão, R.M. Leal, D.M. Rodrigues, Determination of local constitutive

properties of aluminium friction stir welds using digital image correlation, Mater. Des. 33 (2012) 69–74.
[24] W.J. Arbegast, P.J. Hartley, Proceedings of the Fifth International Conference On Trends In Welding Research, Pine Mountain, GA, USA, June 1–5, 1998.
[25] A.N. Albakri, B. Mansoor, H. Nassar, M.K. Khraisheh, Thermo-mechanical and metallurgical aspects in friction stir processing of AZ31 Mg alloy–a numerical and experimental investigation, J. Mater. Process. Tech. 213 (2013) 279–290.
[26] X.X. Zhang, B.L. Xiao, Z.Y. Ma, A transient thermal model for friction stir weld. Part II: effects of weld conditions, Metall. Mater. Trans. A 42A (2011) 3229–3239.
[27] J.H. Yan, M.A. Sutton, A.P. Reynolds, Process-structure-property relationships for nugget and heat affected zone regions of AA2524-T351 friction stir welds, Sci. Technol. Weld. Join. 10 (2005) 725–736.
[28] K.N. Krishnan, On the formation of onion rings in friction stir welds, Mater. Sci. Eng. A 327 (2002) 246–251.
[29] U.F.H.R. Suhuddin, S. Mironov, Y.S. Sato, H. Kokawa, C.-W. Lee, Grainstructure evolution during friction-stir welding of AZ31 magnesium alloy, Acta Mater. 57 (2009) 5406–5418.
[30] W.J. Arbegast, A flow-partitioned deformation zone model for defect formation during friction stir welding, Scr. Mater. 58 (2008) 372–376.
[31] K. Kumar, S.V. Kailas, The role of friction stir welding tool on material flow and weld formation, Mater. Sci. Eng. A 485 (2008) 367–374.
[32] H. Yoshinaga, R. Horiuchi, On nonbasal slip in magnesium crystals, Trans. Jpn. Inst. Met. 5 (1964) 14–21.
[33] R.E. Reedhill, W.D. Robertson, Additional modes of deformation twinning in magnesium, Acta Metall. 5 (1957) 717–727.
[34] S.-G. Hong, S.H. Park, C.S. Lee, Role of {10-12} twinning characteristics in the deformation behavior of a polycrystalline magnesium alloy, Acta Mater. 58 (2010) 5873–5885.